Food chain chaos due to junction-fold point

Bo Deng[a)]
Department of Math and Statistics, University of Nebraska, 810 Oldfather Hall, Lincoln, Nebraska 68588-0323

(Received 19 September 2000; accepted 2 July 2001; published 31 August 2001)

Consideration is given to a basic food chain model satisfying the trophic time diversification hypothesis which translates the model into a singularly perturbed system of three time scales. It is demonstrated that in some realistic system parameter region, the model has a unimodal or logistic-like Poincaré return map when the singular parameter for the fastest variable is at the limiting value 0. It is also demonstrated that the unimodal map goes through a sequence of period-doubling bifurcations to chaos. The mechanism for the creation of the unimodal criticality is due to the existence of a junction-fold point [B. Deng, J. Math. Biol. **38**, 21–78 (1999)]. The fact that junction-fold points are structurally stable and the limiting structures persist gives us a rigorous but dynamical explanation as to why basic food chain dynamics can be chaotic. © *2001 American Institute of Physics.* [DOI: 10.1063/1.1396340]

To understand ecosystem complexity, it is necessary to understand basic food chain dynamics with preys, predators, and top-predators interactions. Chaos has been commonly observed in food chain models by means of numerical simulations. The purpose of this paper is to start a program to classify and analyze chaos generation mechanisms for a basic food chain model. The particular chaos generation mechanism under consideration was also found in models for excitable membranes and neuron cells.[1]

I. INTRODUCTION

An ecosystem is a web of complex interactions among species. Basic food chains can be thought as fundamental building blocks of the web.[2] The chaos theory, which benefited directly from population dynamics[3–5] in its earlier development, is viewed as an important part of a paradigm by which ecocomplexity can be understood. Of the many possible chaotic dynamics in ecology, none is better known than the snowshoe hare and the Canadian lynx system[6] for which a time-delayed phase plot[7] by Ref. 8 suggested a folding structure of the Rössler type[9] that may result in chaotic dynamics. Although a recent time-series analysis by Ref. 10 suggested that the field data[6] may not be chaotic, the implied chaos generating mechanism may still be real and it continues to generate enormous interests among ecologists and applied mathematicians.[11] Nevertheless, there are other ecosystems that we are reasonably sure about their chaoticity based on a collection of different time-series tests on their laboratory and field data.[10] Perhaps a very good reason to study ecochaos, beside the pure intellect pursuit, is due to a recent discovery (which may have important management implications) that the average top-predator biomass in various tritrophic food chain models is maximum at the onset of chaos, see Refs. 12 and 13.

Lotka–Volterra[14,15] models for two species interactions which are spatially homogeneous and time autonomous cannot be more complex than steady states, and limiting cycles. Models for tritrophic chains however are extremely rich in complex dynamics. Perhaps the first numerical work that demonstrated food chain chaos in a tritrophic model was due to Ref. 4. Chaos was also observed in numerical simulations in other tritrophic models.[11–13,16–20] Of which a teacup attractor was discovered in Ref. 16, a strange attractor containing Shilnikov's orbit was found in Ref. 17, and complex homoclinic and heteroclinic orbits were identified and categorized in Refs. 18–20. With progress in classifying elementary bifurcations for both simple and complex orbits and in developing sophisticated numerical packages for detecting and continuing these bifurcations, it is now possible to systematically and numerically map out chaos regions in any parameter space.[16,18–20] The phenomemon of Feigenbaum's period-doubling cascade to chaos[3,21] was a common, often predominant, feature in all these studies. However, due to understandable complexity of tritrophic models there is a lack of understanding in the literature on model mechanisms that are responsible for the period-doubling cascade to chaos. The purpose of this paper is to fill a part of this void by giving a rigorous proof to the existence of period-doubling cascade to chaos scenario in a time-diversified Rosenzweig–MacArthur tritrophic model, which is cast as a singularly perturbed system. The result is obtained at a singular limit. Since singular limiting structures persist in ways considered natural and can be viewed as the origins for the perturbed structures (e.g., Refs. 22–24), this result offers a good explanation to some of the perturbed chaotic dynamics found in the literature (e.g., Refs. 16, 18, 20). The mechanism described should also provide us with a means to interpret nu-

a)Electronic mail: bdeng@math.unl.edu

merical findings some of which can be undecipherable otherwise.

The paper is organized as follows. We will introduce and properly scale the Rosenzweig–MacArthur model in Sec. II. Preliminary analysis is given in Sec. III which provides us with a framework for the period-doubling cascade analysis in Sec. IV. A logistic-type unimodal map is obtained in Sec. IV and a cascade of period-doubling bifurcations is demonstrated when a parameter is varied. This is perhaps the first time that such a map is rigorously found to be embedded in a tritrophic model. Included is also a numerical simulation for the cascade in a parameter region where it is predicted by the theory. Technical analyses are delegated to the Appendix.

II. THE FOOD CHAIN MODEL

In this paper we will consider the Rosenzweig–MacArthur model[25] for tritrophic food chains,

$$\begin{aligned}\dot{x}&=x\left(r-\frac{rx}{K}-\frac{p_1y}{H_1+x}\right),\\ \dot{y}&=y\left(\frac{c_1x}{H_1+x}-d_1-\frac{p_2z}{H_2+y}\right),\\ \dot{z}&=z\left(\frac{c_2y}{H_2+y}-d_2\right).\end{aligned}\tag{2.1}$$

It is composed of a logistic prey (x), a Holling type II predator (y), and a Holling type II top-predator (z). Parameter r is the maximum per-capita growth rate for the prey and K its carrying capacity. Predator's per-capita predation rate has the Holling type II functional form[26]

$$\frac{p_1x}{H_1+x}.$$

Parameter p_1 is the maximum per-capita predation rate and H_1 is the semisaturation constant at which the per-capita predation rate is half of its maximum: $p_1/2$. Parameter c_1 is the maximum per-capita growth rate of the predator. Parameter d_1 is the per-capita natural death rate for the predator. Parameter p_2 and H_2 have similar meanings as p_1 and H_1, except that the predator y is the prey for the top-predator z. Similar explanations also apply to c_2 and d_2. We note that the Rosenzweig–MacArthur model was developed from the seminal works of Lotka[14] and Volterra[15] and is very popular among theoretical ecologists.[16–18,20,27–29]

A. Dimensionless form

With the following changes of variables and parameters,

$$\begin{aligned}&t\to c_1t,\ \ x\to\frac{1}{K}x,\ \ y\to\frac{p_1}{rK}y,\ \ z\to\frac{p_2p_1}{c_1rK}z,\\ &\zeta=\frac{c_1}{r},\ \ \varepsilon=\frac{c_2}{c_1},\ \ \beta_1=\frac{H_1}{K},\ \ \beta_2=\frac{H_2}{Y_0}\quad\text{with}\ \ Y_0=\frac{rK}{p_1},\\ &\delta_1=\frac{d_1}{c_1},\ \ \delta_2=\frac{d_2}{c_2},\end{aligned}\tag{2.2}$$

Eqs. (2.1) are recast in the following dimensionless form:

$$\begin{aligned}\zeta\dot{x}&=x\left(1-x-\frac{y}{\beta_1+x}\right):=xf(x,y),\\ \dot{y}&=y\left(\frac{x}{\beta_1+x}-\delta_1-\frac{z}{\beta_2+y}\right):=yg(x,y,z),\\ \dot{z}&=\varepsilon z\left(\frac{y}{\beta_2+y}-\delta_2\right):=\varepsilon zh(y).\end{aligned}\tag{2.3}$$

Some remarks about the changes of variables and parameters are in order.

The carrying capacity K of the prey is scaled to the dimensionless number 1 by the renormalization, $x\to x/K$. Parameter $Y_0=rK/p_1$ can be interpreted as a predator's predation capacity at which the predator consumes the prey in numbers p_1Y_0 equal to the prey's reproduction capacity rK. This predation capacity is scaled to 1 by the change of variable $y\to y/Y_0$. Similarly, the scaling parameter for the top-predator is

$$Z_0=\frac{c_1Y_0}{p_2},$$

which can be interpreted exactly the same as Y_0 for the predator. That is, since Y_0 is the predation capacity, c_1Y_0 can be interpreted as the predator's reproduction capacity, and Z_0 is the predation capacity for the top-predator at which it consumes the predator in numbers p_2Z_0 equal to predator's reproduction capacity c_1Y_0. This predation capacity for the top-predator is scaled to 1 as well by the renormalization, $z\to z/Z_0$.

Parameters $\beta_1=H_1/K$ is the dimensionless semisaturation constant, measured against prey's carrying capacity, and $\beta_2=H_2/Y_0$ is the dimensionless semisaturation constant for the predator, measured against its predation capacity Y_0. We assume throughout that

$$0<\beta_1<1\ \ \text{and}\ \ 0<\beta_2<1,$$

which can be interpreted to mean that both the predator and the top-predator are good hunters, i.e., capable of reaching half of the maximum predation rates at some population levels smaller than the carrying capacity for the prey and the predation capacity for the predator, respectively.

We also assume throughout that

$$0<\delta_1=\frac{d_1}{c_1}<1\ \ \text{and}\ \ 0<\delta_2=\frac{d_2}{c_2}<1.$$

This is actually a default assumption because the condition of either $\delta_i>1$ would lead to collapse of the tritrophic food chain. More precisely, with $d_1>c_1$, the predator dies out faster than it can reproduce even at its maximum reproduction rate. Therefore both predators will die out as well regardless their initial populations. With $d_2>c_2$, the top-predator must die out by the same reasoning. In either cases we will not have a nontrivial tritrophic food chain, whose dynamics are completely understood.

B. Tritrophic time diversification hypothesis

A reasonable assumption to make is to assume the ''trophic time diversification hypothesis'' which states that *the maximum per-capita growth rate decreases from bottom to top along the food chain*, namely,

$$r>c_1>c_2>0.$$

In this paper, we actually assume a drastic time diversification

$$r\gg c_1\gg c_2>0 \quad \text{or equivalently}$$
$$0<\zeta\ll 1 \quad \text{and} \quad 0<\varepsilon\ll 1. \tag{2.4}$$

Under this condition, Eqs. (2.3) become a singularly perturbed system of three time scales. The rates of change for the prey, predator, and top-predator range from fast to intermediate to slow, respectively. Three-time-scale trophic models were introduced in Ref. 27. They took the same form as Eq. (2.1) except that $\dot{y}$, $\dot{z}$ were replaced by $\epsilon\dot{y}$, $\epsilon^2\dot{z}$, respectively for a small time scaling factor $\epsilon>0$. Our changes of variables and parameters as in (2.2) together with $\zeta=\varepsilon$ produce the same time-diversified models as in Ref. 27, of course under appropriate readjustments on other parameters.

We note that the period-doubling cascade to chaos is to be found at the singular limit $\zeta=0$.

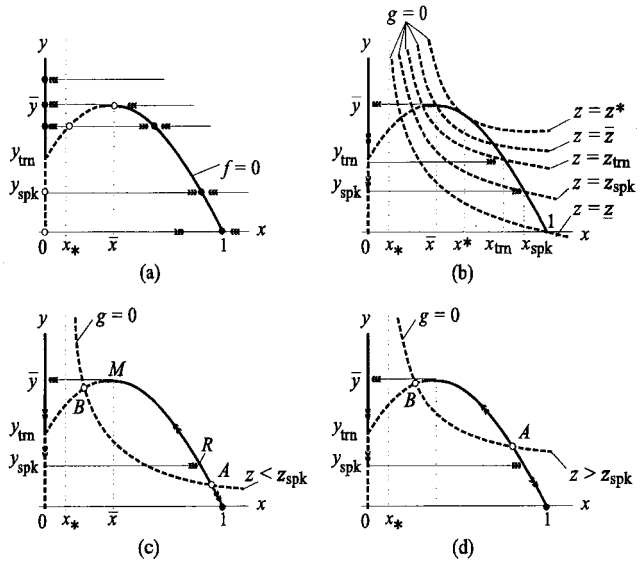

FIG. 1. (a) x-phase lines and the x-nullcline surfaces $x=0$ and $f=0$ for the fast subsystem. Points of $x=0, y_{\rm trn}<y$ and $f(x,y)=0,\bar{x}<x$ are the only stable equilibrium points. (b) The type of y-nullclines that is considered in this paper. (c) Singular relaxation cycle $RM\bar{y}y_{\rm spk}$ for the predator–prey subsystem. (d) The cycle disappear through the bifurcation $z=z_{\rm spk}$. Solid nullclines are for attracting equilibrium manifolds and dash nullclines are for unstable equilibrium manifolds.

III. FAST-INTERMEDIATE-SLOW ANALYSIS

Because of the ways the two small parameters $0<\zeta\ll 1, 0<\varepsilon\ll 1$ appeared in Eqs. (2.3), we are dealing with a three-time-scale system. Such multitime scaled systems can be analyzed by reducing the full three-dimensional dynamics to two dimension first and then to one dimension, under some appropriate conditions, see, e.g., Refs. 27–30. An elementary tutorial can be found in Ref. 30. The key lies in our understanding about the nullcline surfaces $xf(x,y)=0, yg(x,y,z)=0, zh(y,z)=0$. We note that all discussions below are confined to the first quadrant $x\geqslant 0, y\geqslant 0, z\geqslant 0$.

A. Prey dynamics: Fast

By rescaling the time $t\to t/\zeta$ for Eq. (2.3) and setting $\zeta=0$ for the new equations, we obtain the fast prey subsystem,

$$x'=xf(x,y), \quad y'=0, \quad z'=0.$$

It is one-dimensional and its flow is completely determined by its equilibrium surface $xf(x,y)=0$, which is composed of $x=0$ and $f(x,y)=0$. The surface $f(x,y)=0$ is a cylindrical parabola,

$$y=(1-x)(\beta_1+x).$$

It has its maximum point and maximum value as

$$\bar{x}=\frac{1-\beta_1}{2}, \quad \bar{y}=\frac{(1+\beta_1)^2}{4}. \tag{3.1}$$

It intersects the trivial equilibrium surface $x=0$ at

$$y=y_{\rm trn}=\beta_1 \tag{3.2}$$

(see Figs. 1 and 2).

The fast dynamics is determined depending the value of y. For any fixed $0\leqslant y\leqslant y_{\rm trn}$, the trivial equilibrium point $x=0$ is unstable, and the nontrivial one on the slow manifold $f=0$ is stable. In addition, for the same range $0\leqslant y\leqslant y_{\rm trn}$, all fast orbits converge to the latter with initial value $x_0>0$. On the other hand, for $y_{\rm trn}\leqslant y\leqslant\bar{y}$, there are three equilibrium points. The trivial solution $x=0$ is stable, the middle one on the parabola $f=0$ between $0\leqslant x\leqslant\bar{x}$ is unstable, and the one on the right branch of the parabola $f=0$ is stable. For $y>\bar{y}$, $x=0$ is the only equilibrium point which is globally

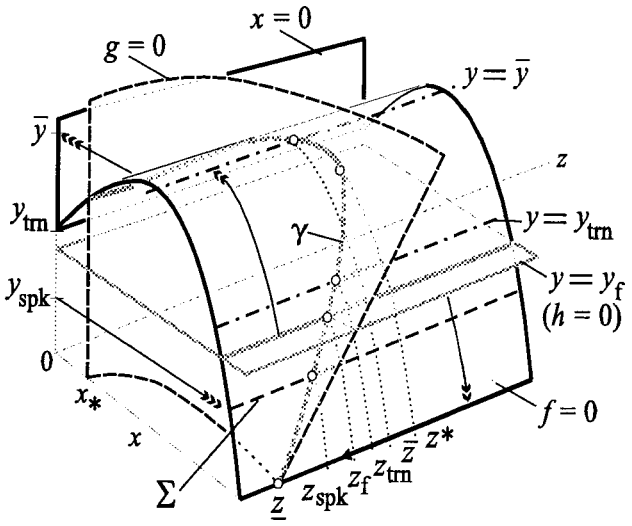

FIG. 2. Nullcline surfaces drawn in the full three-dimensional phase space. The jump from the fold $y=\bar{y}$, $x=\bar{x}$ to the x-stable part of the manifold $x=0$ in direction of x is the fastest. The crawl on the x-stable part of the parabola $f=0$ in the direction of y is slow comparing to the x-fast jump but fast comparing to the slow drift in the z-direction.

stable. Thus, $y=\overline{y}$ is a fold bifurcation point (or saddle-node bifurcation point) for the fast prey system, and $y=y_{\rm trn}$ is a transcritical bifurcation point (see Figs. 1 and 2).

B. Predator dynamics: Intermediate

Setting $\zeta=\varepsilon=0$ in Eq. (2.3) gives rise to the predator subsystem

$$xf(x,y)=0,\dot{y}=yg(x,y,z),\dot{z}=0, \tag{3.3}$$

which has the intermediate time scale. Orbits of this subsystem lie either on the trivial manifold $x=0$ or on the parabola $f(x,y)=0$ with variable z frozen at a constant.

Again, the intermediate prey dynamics is determined by its equilibrium states $y=0$ and $g=0$, in particular the stable equilibrium states. The intermediate orbits develop upwards if $g>0$ and downwards if $g<0$. Figure 1(b) illustrates several y-nullcline curves $g=0$ that define many parameter-dependent variable values we will use throughout the paper. Since f is independent of z, these $g=0$ curves are plotted against one parabola $f=0$. Notice that the variable y can be solved from $g=0$ to get

$$y=-\beta_2+z\Big/\left(\frac{x}{\beta_1+x}-\delta_1\right) \quad \text{if} \quad g=0.$$

It decreases in x and increases in z. Thus, the nullcline curve $g=0$ of a higher value of z lies above the nullcline curve $g=0$ of a lower value of z. With the value $y_{\rm spk}$ to be explained below, the corresponding y-nullcline $g(x,y,z_{\rm spk})=0$ with $z=z_{\rm spk}$ shown in Fig. 1(b) has the property that it intersects both the stable and the unstable branches of the parabola $f=0$. This property is equivalent to that the y-nullcline $g(x,y,\overline{z})=0$ with $z=\overline{z}>z_{\rm spk}$ intersects the x-stable branch of the parabola $f=0$ at a y-level higher than $y=y_{\rm spk}$, in addition to its intercept with the maximum point $(\overline{x},\overline{y})$ of the parabola. We note that the configurations of Fig. 1(b) correspond to the kind of parameter region under consideration and the relationship between them will be determined throughout the discussion and mostly in the Appendix.

C. Relaxation oscillations in predator–prey

With each z fixed in the predator subsystem (3.3) we have a singular limiting system in the predator and prey. The perturbed system (2.3) with $0<\zeta\ll 1$ and $\varepsilon=0$ is well approximated by the singular predator–prey Eqs. (3.3) (e.g., Ref. 22). Three cases need to be distinguished: $0\leqslant z<z_{\rm spk}$, $z=z_{\rm spk}$, and $z>z_{\rm spk}$.

Figure 1(c) illustrates the case of $0\leqslant z<z_{\rm spk}$. On the trivial manifold $x=0$, the intermediate y-dynamics has only one equilibrium point $y=0$, which is stable. On the parabola manifold $f=0$, it has three equilibrium points, labeled 1, A, B. A, B are unstable and 1 is stable. It is important to notice that for $0\leqslant z<z_{\rm spk}$, the saddle point A lies below the plane $y=y_{\rm spk}$.

A typical intermediate orbit in this case behaves like this: If it starts on $f=0$ and from, say, the point R, it crawls upwards. When it reaches the fold point M, it jumps instantaneously, or is concatenated by a fast x-orbit, to the x-attracting trivial manifold $x=0$ and lands at a point $\overline{y}$ from which a new intermediate y-orbit on $x=0$ develops downwards, heading to the stable equilibrium point $y=0$. It must cross the transcritical point $y_{\rm trn}$ and stay on $x=0$ for awhile until reaching a point $y_{\rm spk}$. At this point $y_{\rm spk}$, the intermediate segment encounters a phenomenon referred to as *Pontryagin's delay of lost stability*,[22,28,31,32] and see more explanation below. Simply put, the theory says that the intermediate y-orbit must be concatenated by a fast x-orbit from the point $y_{\rm spk}$ on $x=0$ to the point $y_{\rm spk}$ on the parabola x-equilibrium manifold $f=0$, which is the point R. Since R is where the first intermediate y-orbit started, the concatenated fast and intermediate singular orbits form a cycle $RM\overline{y}y_{\rm spk}$, representing a relaxation oscillation for the predator–prey interaction with any frozen $0\leqslant z<z_{\rm spk}$. Also, for any point started above the plane $y=A$ and away from $x=0$, the predator–prey singular orbit is always attracted to the singular cycle. That is, the basin of attraction of the singular cycle is $\{x>0,y>A\}$. However, for any orbit started below the plane $y=A$ and away from $x=0$, it is attracted to the stable equilibrium point $y=0$ with $x=1$.

In the second case with $z=z_{\rm spk}$, the predator–prey singular cycle $RM\overline{y}y_{\rm spk}$ is interrupted by the saddle point A, a singular homoclinic orbit is formed. It is a point of bifurcation. For the third case with $z>z_{\rm spk}$, illustrated in Fig. 1(d), the singular cycle is gone. Every point with a nonvanishing initial x value is attracted to the equilibrium point $x=1$ and $y=0$.

D. Pontryagin's delay of lost stability

The point of Pontryagin's delay of lost stability $y_{\rm spk}$ is determined by the following integral:[22,28,31,32]

$$\int_{y_{\rm spk}}^{\overline{y}}\frac{f(0,\xi)}{\xi g(0,\xi,z)}d\xi=0, \tag{3.4}$$

with each given value of z. Although the integration is elementary, the equation for $y_{\rm spk}$ is transcendental. Nevertheless, the function $y_{\rm spk}(z)$ can be proven to be decreasing in z.[28] One intuitive explanation (e.g., Ref. 30) to why the intermediate orbit does not jump at the transcritical point $y=y_{\rm trn}$ instead at $y=y_{\rm spk}$ goes as follows. In a ζ-neighborhood of the point $(0,y_{\rm trn})$, both x and f are order ζ so that $\dot{x}$ is order ζ and $\dot{y}$ is order 1. It develops further downwards until both x and f is order 1 so that $\dot{x}$ is order $1/\zeta$ to initiate the jump. Pontryagin's theory says two things. First, any perturbed predator–prey orbit Γ_ζ with initials having $y=\overline{y}$, $0<\zeta\ll 1,\varepsilon=0$, Γ_ζ has limit Γ_0 as $\zeta\to 0$, and the limit Γ_0 is the concatenated fast and intermediate orbit described above, having a Pontryagin turning point at $(0,y_{\rm spk})$. Second, the theory says that the turning point depends on the initial value in y. Qualitatively, the farther away from the transcritical point $y_{\rm trn}$ the initial y-value is, the farther down below it the Pontryagin turning point locates.

E. Top-predator dynamics: Slow

The top-predator dynamics is determined by the z-nullcline which is the union of $z=0$ and $h(y)=0$. The equation $h(y)=0$ defines a plane

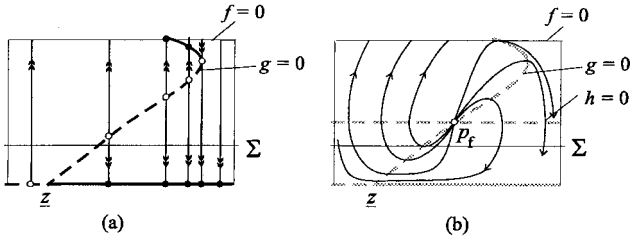

FIG. 3. Phase portraits for the reduced vector field on the x-stable branch of the parabola $f=0$. (a) $\varepsilon=0$; (b) $0<\varepsilon\ll 1$.

$$y=y_f:=\frac{\delta_2\beta_2}{1-\delta_2} \tag{3.5}$$

parallel to the (x,z)-plane, see Fig. 2. Above the plane the top-predator population $z(t)$ decreases, and below the plane, $z(t)$ increases.

F. Predator-top-predator interaction on $f=0$

On the x-stable branch of the parabola $f=0$, the intermediate-slow dynamics

$$xf(x,y)=0,\ \dot{y}=yg(x,y,z),\ \dot{z}=\varepsilon zh(y)$$

is only two-dimensional. Its vector field and phase portrait can be easily described. Figure 3 is a phase portrait. Figure 3(a) is for the case $\varepsilon=0$, in which the portrait consists of phase lines parameterized by the z-variable, with the y-nullclines $y=0$ and $g=0$ determining the directions of the phase line flows. For small $0<\varepsilon\ll 1$, the phase lines of Fig. 3(a) are no longer vertical lines because of the slow drift in the z-variable. They become solution curves of the two-dimensional predator-top-predator system on the manifold $f=0$ as illustrated in Fig. 3(b). The intermediate-slow orbits must cross the y-nullcline $g=0$ *horizontally* and the z-nullcline $h=0$, or $y=y_f$ *vertically*. Above the z-nullcline $y=y_f$, they move to the right, and below the line, they move to the left. Right of the y-nullcline $g=0$, they move down, and left of it, they move up. With the configuration $\underline{z}<z_{\rm spk}<\bar{z}$ under consideration, the equilibrium point $p_f=(x_f,y_f,z_f)$ is a source on $f=0$ as shown. The equilibrium point can become a sink with some other configurations of the predator and top-predator nullclines.[27]

In comparison, we note that the predator-top-predator interaction on the trivial x-nullcline surface $x=0$ is simpler: All orbits develop downward and encounter their Pontryagin turning points.

G. Bursting-spiking phenomenon

Some typical scenarios are worth mentioning here for the perturbed system with $\zeta=0, 0<\varepsilon\ll 1$. Suppose a singular orbit is started at (x_0,y_0,z_0) which is on the x-stable branch of the parabola $f=0$ and to the right of the y-unstable branch of the curve $\gamma=\{g=0\}\cap\{f=0\}$. Then the fast-intermediate singular segment moves quickly to the y-stable branch $x=1$, $y=0$, $z>\underline{z}$. Once it is near that slow segment, it moves in the decreasing direction of z as it is below the z-nullcline plane $y=y_f$. There is little change in the prey x and the predator y populations. The point $\underline{z}$ is a transcritical point for the slow z-equation. The Pontryagin theory described above again applies. Thus, the slow singular orbit will first cross the point $\underline{z}$, stay along the y-unstable branch $x=1$, $y=0$, $z<\underline{z}$ for awhile until reaching a Pontryagin turning point $z_p(z_0)$, at which the intermediate singular orbit in y takes over. The subsequent fast-intermediate-slow development of the orbit is almost exactly the same as in the case of Fig. 1(c), with possible exceptions that the fast-intermediate relaxation oscillation may not close on itself since the variable z is not frozen. It is easy to see that if the z-nullcline plane $h=0$, which is $y=y_f$, lies below $y=y_{\rm spk}$ (i.e., $y_f<y_{\rm spk}$), then the fast-intermediate cycles stay above the plane $y=y_f$ and therefore will form a train of cycles that moves with ever increasing value in z, and eventually enter the region right of the y-nullcline $g=0$. By a train of cycles we mean there are no fewer than two cycles riding on the orbit before entering the region $\{g(x,y,z)<0\}$, see, e.g., Fig. 5(d). Notice that once the spike train enters the region $\{g(x,y,z)<0\}$, the spikes must eventually be terminated as all intermediate-slow orbits on $f=0$ head down to the y-stable branch $x=1$, $y=0$, $z>\underline{z}$ again. Also, a spike train always forms for sufficiently small $0<\varepsilon\ll 1$ because the predator–prey oscillation is much faster than the top-predator evolution whose rate of change is only order ε. This phenomenon of fast spike trains punctuated with quiescent phases is called bursting-spiking in the context of neuronal dynamics, see, e.g., Refs. 1 and 33. For y_f slightly above $y_{\rm spk}$, the same bursting-spiking phenomenon may occur as the train progresses towards $z=z_{\rm spk}$ by spending more time in the region above $y=y_f$ than below it. Bursting-spiking phenomenon was discovered in neuronal dynamics, long before being recognized and analyzed for the Rosenzweig–MacArthur food chain model.[16,18,20,27,29]

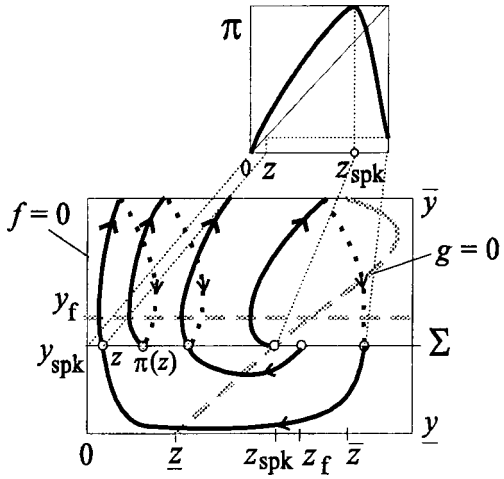

FIG. 4. Projected phase portraits onto the (y,z)-plane. Oriented solid curves are the intermediate-slow orbits on the x-stable parabola $f=0$ and those of dotted ones are the the intermediate-slow orbits on the trivial manifold $x=0$. A point of return takes exactly one solid intermediate-slow orbit on the parabola and one dotted intermediate-slow orbit on $x=0$ to complete. The fast jump from a solid to a dotted takes place at the fold line $y=\bar{y}$, whereas the jump from a dotted to a solid takes place along the Pontryagin delay of stability curve $y=y_{\rm spk}$ which is a function of both ε and z. The inserted diagram is a schematic for the unimodal return map.

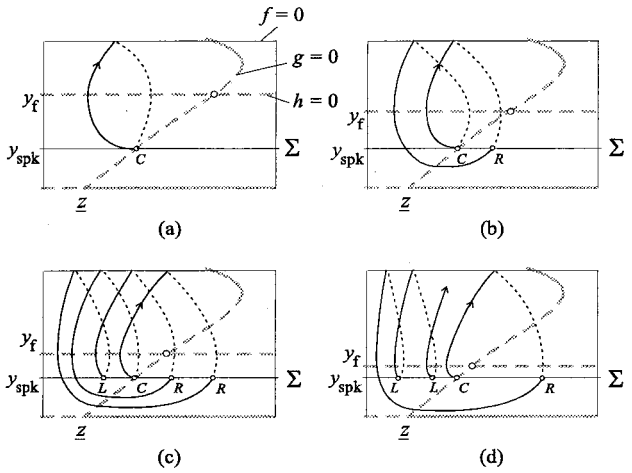

FIG. 5. (a) A 1-cycle of kneading sequence C. (b) A period-2 cycle of kneading sequence RC. (c) A period-4 cycle of kneading sequence of $RLRC$. (d) A bursting-spiking orbit of kneading sequence $RLL\cdots$. The y_f ranges from high to low, giving rise to a reversed period-doubling cascade bifurcation.

The question of how the orbit will behave after entering the region $z>z_{\rm spk}$ leads to the main discussion of the next section as to how chaotic dynamics and period-doubling cascade take place in the parameter region defined by the following relation:

$$\underline{z}<z_{\rm spk}<z_f<\overline{z}. \tag{3.6}$$

Proposition 6.5 of the Appendix gives a set of sufficient parameter constraints that guarantees the relation above.

We conclude this section by pointing out that for parameter values which make $y_f=y_{\rm spk}$, singular homoclinic orbit may occurs if the relaxation oscillation train originated from the equilibrium point (x_f,y_f,z_f) returns and hits precisely itself. This type of homoclinic orbits can be degenerate if it arises from the strong unstable manifold of the equilibrium point. (The strong unstable manifold at the limit $\varepsilon=0$ is simply $z=z_f$.) It was pointed out in Ref. 34 that the existence of such an orbit can lead to complex dynamics in a vicinity of the orbit. The existence of such orbits for the food-chain model was first demonstrated geometrically in Ref. 30. Our remark above follows the spirit of that paper. Studying food chain dynamics from the view of homoclinic and heteroclinic orbits can also be found in Refs. 18–20.

IV. PERIOD-DOUBLING CASCADE

A. Junction-fold point

We begin with a few remarks about the Pontryagin delay of stability at the transcritical point $y=y_{\rm trn}$. We pointed out in the previous section that for $\zeta=\varepsilon=0$ and with any frozen value $z\geqslant 0$, the intermediate orbit segment starting at $y=\overline{y}$ on $x=0$ moves down and initiates an instantaneous jump at point $y=y_{\rm spk}$. The value $y_{\rm spk}$ is a function of $z\geqslant 0$, decreasing in z by Ref. 28. By the singular perturbation theory,[22,31,32] this curve can be continued for $0\leqslant\varepsilon\ll 1$, with $\zeta=0$. We denote by Σ the curve that the fast x-orbits land on the x-stable part of the parabola $f=0$ concatenated from the Pontryagin turning curve $y=y_{\rm spk}$, see Fig. 2. We will call it *the junction curve*.

By Proposition 6.6 of the Appendix, the junction curve Σ and the intermediate-slow vector field on $f=0$ with $\varepsilon>0$ has this important property: in a parameter region there is a unique point, denoted by $p_{\rm spk}=(x_{\rm spk},y_{\rm spk},z_{\rm spk})$ and referred to as *the junction-fold point*,[1,24] such that for any point $p\in\Sigma$ left of $p_{\rm spk}$, the intermediate-slow vector field in (y,z) on $f=0$ points above Σ whereas for any point on Σ and right of the junction-fold $p_{\rm spk}$ it points below Σ. In other words, $p_{\rm spk}$ is the only point on Σ at which the perturbed intermediate-slow vector field with $0<\varepsilon\ll 1$ has a quadratic-like tangent to Σ.

B. Unimodal return map

We are now ready to examine singular orbits with $\zeta=0,0<\varepsilon\ll 1$ that are originated from the junction curve Σ. We simplify the illustration by viewing the x-stable part of the parabola $f=0$ in terms of its projection to the yz-plane as in Fig. 4 and exam the three-species interactions on the two-dimensional projection. In this way the fast jumps in the prey x-dynamics are either going into the page from the fold $y=\overline{y}$ to $x=0$ or out of it from the Pontryagin turning point $y=y_{\rm spk}$ on $x=0$ to the junction curve Σ on the parabola $f=0$. Since $y_{\rm spk}$ is a decreasing function of $z\geqslant 0$, we can parameterize Σ by the z variable, and suffice to denote points on Σ by their z-values.

The parameter region that is under consideration is defined by (3.6), i.e.,

$$\underline{z}<z_{\rm spk}<z_f<\overline{z}.$$

There are two distinct cases to consider: Points left of the junction-fold: $z<z_{\rm spk}$ and points right of the junction-fold: $z>z_{\rm spk}$. The condition $z_{\rm spk}<z_f$, equivalently $y_{\rm spk}<y_f$, plays an important role in the discussion below.

If $z<z_{\rm spk}$, the intermediate-slow orbit (solid curve) on the parabola $f=0$ moves upwards away from Σ. Drift left first because it is below $y=y_f$; cross $y=y_f$ vertically; and then drift right because it is above $y=y_f$. Since $\overline{z}>z_{\rm spk}$, it must hit the turning fold $\{y=\overline{y}\}$ strictly left of $\overline{z}$ for small $\varepsilon>0$. Continuity is the reason, because for $\varepsilon=0$ the intermediate singular orbit will hit the fold $y=\overline{y}$ at exactly the same frozen $z=$constant value strictly left of $z_{\rm spk}<\overline{z}$, see Fig. 3(a). Therefore the relation $z<z_{\rm spk}<\overline{z}$ on the fold $y=\overline{y}$ will be preserved for the orbit when $\varepsilon>0$ is sufficiently small, see Fig. 3(b). We note that $z=\overline{z}$ for $\varepsilon=0$ is a *canards* point[35,36] for the predator–prey subsystem. This point is not made accessible to any orbit originated from the junction curve Σ by the condition $z_{\rm spk}<\overline{z}$. Hence, once the orbit reaches the fold $y=\overline{y}$, it is joined by a fast x-orbit to the plane $x=0$. On $x=0$, another intermediate-slow orbit (dotted curve on $x=0$) takes over and moves down until it reaches its Pontryagin turning point $y=y_{\rm spk}$. At that point, it is taken over by another instantaneous jump in x to the junction line Σ and the point this concatenated singular orbit lands is denoted by $\pi(z)$. In this manner we have defined a one-dimensional Poincaré return map π.

For junction points right of the junction-fold $z>z_{\rm spk}$, the description for the Poincaré return map is somewhat different. Again, the relation $y_{\rm spk}<y_f$ plays the determinant role. First all intermediate-slow orbits originated right of the junction-fold move left and below Σ. Each of them must cross *horizontally* on the y-nullcline $g=0$ in a manner that the crossing is continuously dependent of the initial point and is continuously extendable to include $z=z_{\rm spk}$ at which both the initial and the crossing points coalesce. After its crossing, it moves up and leftwards until it crosses the junction curve Σ from below and *left* of the junction-fold point $z_{\rm spk}$. After this crossing, it then moves in exactly the same way as described above for points left of the junction-fold $z_{\rm spk}$ and returns to Σ by a concatenated singular orbit. In this way, we define the Poincaré return $\pi(z)$ for $z>z_{\rm spk}$.

The inset of Fig. 4 shows a schematic of the map $\pi:\Sigma\to\Sigma$. It is important to point out that for $0<\varepsilon\ll 1$, the return map π is continuous based on the continuity property of the intermediate-slow orbits on their initial conditions. More specifically, it is continuously differentiable at any point $z\neq z_{\rm spk}$ because the intermediate-slow vector field is transversal to Σ at such a point. At $z=z_{\rm spk}$, the vector field is tangent to Σ. Although the transversality-implies-differentiability argument does not apply to this point, one can still show by an elementary calculus argument that π is also differentiable at $z=z_{\rm spk}$ and the derivative is 0, so long as the tangency of the vector field to Σ at $z_{\rm spk}$ is quadratic-like. (For a proof of this fact, see Ref. 1.) Though obvious, it is important to point out that the map is unimodal, i.e., increasing in the left interval $z<z_{\rm spk}$ and decreasing in the right interval $z>z_{\rm spk}$.

C. Kneading sequences and period-doubling cascade

The most important property pertinent to a period-doubling cascade to chaos is the following. If the z-nullcline $y=y_f$ is just slightly above the junction curve $\Sigma, y=y_{\rm spk}$, then leftward drift by the intermediate-slow orbits below the plane $y=y_f$ is small comparing to its rightward drift above the plane $y=y_f$ on both the parabola $f=0$ and the plane $x=0$. Therefore $\pi(z)>z$ for $z<z_{\rm spk}$, see Fig. 4. In particular, this also holds for the critical point $\pi(z_{\rm spk})>z_{\rm spk}$. If, however, the parameter value y_f, which defines the z-nullcline $y=y_f$, increases sufficiently above $y_{\rm spk}$ so that the leftward drift cannot compensate the rightward drift, then the relation $\pi(z_{\rm spk})>z_{\rm spk}$ will be reversed to $\pi(z_{\rm spk})\leqslant z_{\rm spk}$. In other words, as y_f increases away from $y_{\rm spk}$, the maximum point of π moves down and crosses the diagonal $\pi=z$. This is, in a reversed manner, very similar to the logistic map $x\to\lambda x(1-x)$ when it goes through the period-doubling cascade as its maximum point $(1/2,\lambda/4)$ moves through the diagonal with λ going through 2.

This reversal for our map π signals a qualitative change or bifurcation in the kneading sequence of the unimodal map between parameter values for which y_f is just slightly above $y_{\rm spk}$ and parameter values for which y_f is sufficiently above $y_{\rm spk}$.

By definition, the kneading sequence of a unimodal map is *the itinerary* of the orbit $\{z_0,z_1,z_2,\dots\}$ with the initial point $z_0=\pi(z_{\rm spk})$, and $z_{i+1}=\pi(z_i)$. The critical point $z_{\rm spk}$ is denoted by the symbol C for its itinerary. Any point right of the critical point $z_{\rm spk}$ is designated by the itinerary symbol R whereas any point left of it is denoted by the symbol L. For example, if $\pi(z_{\rm spk})=z_{\rm spk}$, then the kneading sequence is just $CC\cdots$, see Fig. 5(a). In this case, y_f is sufficiently greater than $y_{\rm spk}$ as described above. On the other hand, if y_f is just slightly greater than $y_{\rm spk}$ so that the rightward drift of the singular orbit from $z_{\rm spk}$ is far greater than the leftward drift, resulting the return point $\pi(z_{\rm spk})$ on Σ significantly farther right of the critical point $z_{\rm spk}$, see Figs. 5(b)–5(d). The first itinerary symbol is thus an R. The next return point $\pi^2(z_{\rm spk})$ can be left of $z_{\rm spk}$ precisely because the first iterate $\pi(z_{\rm spk})$ is farther right of $z_{\rm spk}$. To see this, notice that $z=0$ is the other z-nullcline. Thus the change in z is slower when nearer the plane $z=0$ than father away from it. Therefore, if $\pi^2(z_{\rm spk})$ is sufficiently near $z=0$, the next iterate $\pi^3(z_{\rm spk})$ will still be to the left of the critical point $z_{\rm spk}$, giving rise to a spike train. In other words, the two subsequent itinerary symbols can both be L, and the kneading sequence may take the form $RLL\cdots$, see Fig. 5(d).

According to the kneading sequence theory [e.g., for a general treatment[37] and for a tailored treatment,[1] respectively], the kneading sequence difference between being $CC\cdots$ and $RLL\cdots$ along a one-parameter path in the parameter space is sufficient to result in a cascade of period-doubling to chaos along the one-parameter path, which corresponds to driving y_f down and toward $y_{\rm spk}$ in our case. (See more detailed discussion below, as well as the Appendix and Ref. 1.) Figure 5 illustrates part of the cascade with various configurations in $y_{\rm spk}$ and y_f that give rise to period-1, -2, -4 orbits going through the critical point. The kneading sequences in these three cases are $CC\cdots$, $RC\overline{RC}$, and $RLRC\overline{RLRC}$. Figure 5(d) illustrates a bursting-spiking orbit whose kneading sequence takes the form $RLL\cdots$.

The only question left now is in what parameter region does the described kneading sequence bifurcation occur.

D. Parameter region for the cascade

We note first that parameter δ_2 is special. It appears only in the top-predator equation. Therefore it does not appear in neither the x-nullcline manifold $f=0$ nor the y-nullcline manifold $g=0$. Hence the parameter values $\underline{z}$, $z_{\rm spk}$, $\overline{z}$ from the relation (3.6) that defines the region of our discussion do not depend on δ_2. Second, we note that by Proposition 6.5 of the Appendix there is a function $b(\beta_1,\delta_1)$ satisfying $b\to\infty$ as $\beta_1\to 0$ so that the following part of the relation (3.6),

$$\underline{z}<z_{\rm spk}<\overline{z} \tag{4.1}$$

holds if

$$0<\beta_1<\tfrac{1}{3},\ \ 0<\delta_1<\frac{1-3\beta_1}{1-\beta_1},\ \text{ and }\ 0<\beta_2<b(\beta_1,\delta_1).$$

Therefore, to ensure relation (3.6), we only need to ensure

$$z_{\rm spk}<z_f<\overline{z}. \tag{4.2}$$

This is where the parameter δ_2 plays an important role.

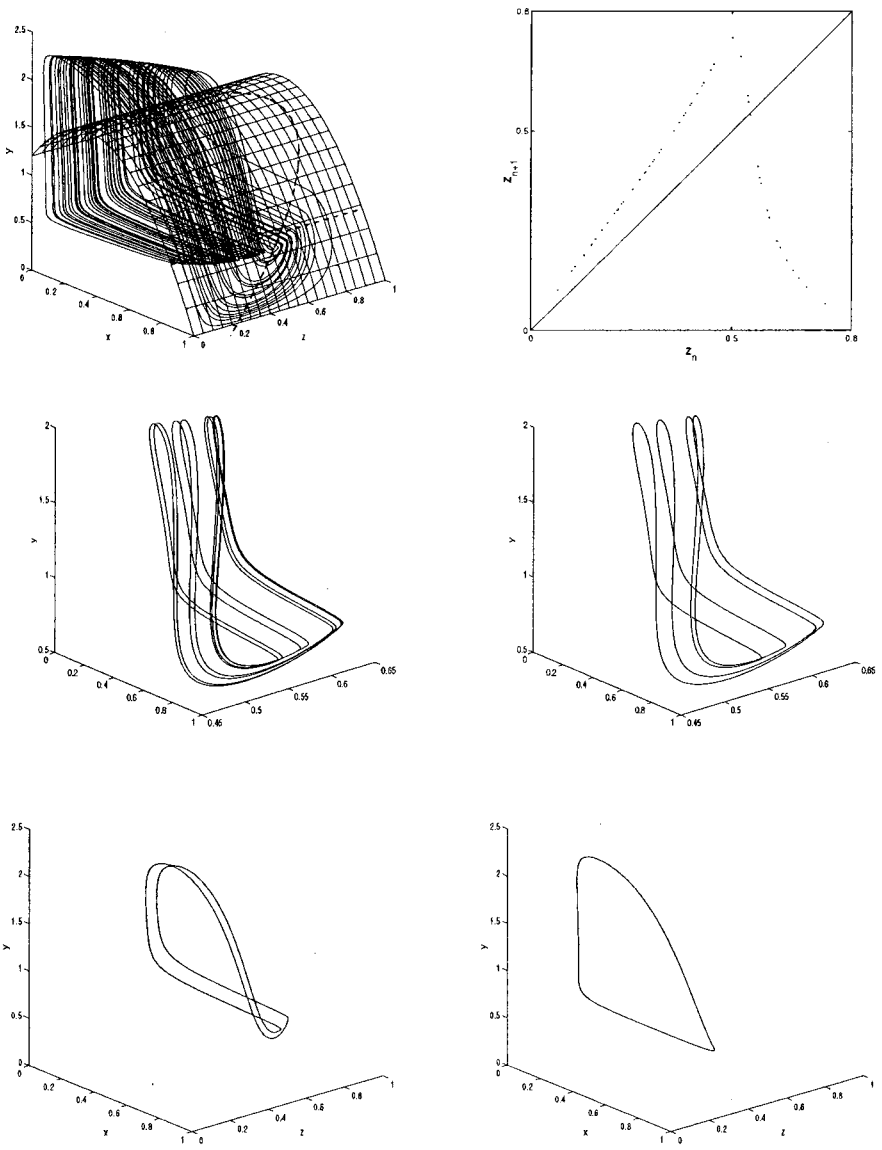

FIG. 6. A chaotic attractor for $\delta_2 = 0.62$ in the top-left figure. The curve γ and the z-nullcline on $f=0$ are the dash curves. The top-right figure is the z-projection of the Poincaré return map which is shown to be close to the one-dimensional, limiting Poincaré map. The remaining figures show that the system goes through a reversed period-doubling cascade for parameter values $\delta_2 = 0.677\,85, 0.678\,23, 0.68, 0.7155$ for period 8, 4, 2, 1 orbits, respectively.

By Proposition 6.2 of the Appendix a point (x,y,z) from the y-nullcline curve $\gamma=\{g=0\}\cap\{f=0\}$ has the property that increase in z in the interval $[\underline{z},\overline{z}]$ corresponds to increase in y in the corresponding interval $[\underline{y},y^*]$. Therefore, the required relation $z_{\rm spk}<z_f$ is equivalent to $y_{\rm spk}<y_f$ for which $y_f=\delta_2\beta_2/(1-\delta_2)$ from the z-nullcline Eq. (3.5). Solving the inequality $y_{\rm spk}<\delta_2\beta_2/(1-\delta_2)$ we have that in order for $z_{\rm spk}<z_f<\overline{z}$ to hold it is sufficient to have

$$\delta_2>\beta_0 := \frac{y_{\rm spk}}{y_{\rm spk}+\beta_2}. \tag{4.3}$$

This relation can always be obtained by changing the value of δ_2 because $y_{\rm spk}$ does not depend on δ_2.

In conclusion, relation (4.1) always holds for sufficiently small β_1. Once that part of (3.6) is secured, we can increase δ_2 so that (4.3) holds, thus making the remaining part (4.2) of (3.6) hold. In other words, as we increase δ_2 through the point $\beta_0=y_{\rm spk}/(y_{\rm spk}+\beta_2)$, the maximum point of the Poincaré return map π will change from $\pi(z_{\rm spk})>z_{\rm spk}$ to $\pi(z_{\rm spk})\leqslant z_{\rm spk}$, not at the value $\delta_2=\beta_0$ but at some greater value $\delta_2>\beta_0$. As we concluded in the previous section that this reversal only creates a condition necessary for a period-doubling cascade to occur and that we also need the kneading sequence to be $RLL\cdots$ for δ_2 just slightly above β_0 so that a cascade does occur.

This is where the parameter $0<\varepsilon\ll 1$ comes in to satisfy the kneading sequence conditions. For the type of singular Poincaré return maps π that arise from three-time-scale singularly perturbed systems such as Eq. (2.3), it was estimated quantitatively in Ref. 1 that within an order of $y_f-y_{\rm spk}=\mathcal{O}(1/|\ln\varepsilon|)$, not only $\pi(z_{\rm spk})$ will change from $\pi(z_{\rm spk})>z_{\rm spk}$ to $\pi(z_{\rm spk})<z_{\rm spk}$ but also this change will give rise to the required kneading sequence bifurcation from $RLL\cdots$ to $C\overline{C}$, therefore guaranteeing the period-doubling cascade to take place. Because of this order estimate and the fact that $\overline{y}-y_{\rm spk}=\mathcal{O}(1)$ and $\beta_0<1$, the transition is guaranteed for $\beta_0<\delta_2<1$ and sufficiently small $0<\varepsilon\ll 1$. In other words, the transition is completed for sufficiently small $0<\varepsilon\ll 1$ far before y_f hits its definition limit $\overline{y}$ or equivalently before δ_2 hits its definition limit 1. These facts are established in Theorem 6.1 in the Appendix.

We also point out that there is this chaotic point at which the period-doubling cascade sequence converges and many other complex points such as period-three points during the transition, typical of the logistic map.

E. Numerical simulation

In theory we should look for the period-doubling cascade at the singular limit $\zeta=0$ and with the condition $\delta_2>\beta_0$. We should also expect the cascade to persist for $0<\zeta\ll 1$. In fact, near the junction-fold point $p_{\rm spk}$, the perturbed map becomes a two-dimensional horseshoe-like map as proven in Sec. IV of Ref. 1 (see Fig. 4.1 of the reference). For $\zeta>0$, however, we should actually expect the cascade for $\delta_2\approx\beta_0$, and more likely $\delta_2\leqslant\beta_0$. The reason is two-fold. First, for $\zeta>0$, orbits coming from a neighborhood of the x-stable part of the parabola $f=0$ commence the first fast jump at points higher than the fold $y=\bar{y}$ and therefore the second jump at points lower than the curve of Pontryagin's delay of lost stability $y=y_{\rm spk}$. That in turn lowers the actual junction line Σ. As a result, $\{y=y_f\}$ crosses the "perturbed" junction line at a lower value of δ_2.

Figure 6 consists of some numerical simulations for the system with parameter values $\zeta=0.1$, $\varepsilon=0.4$, $\beta_1=0.3$, $\beta_2=0.1$, $\delta_1=0.1$, and various parameter values of δ_2. The predicted transition at $\zeta=0$ should start above $\delta_2=\beta_0=y_{\rm spk}/(y_{\rm spk}+\beta_2)$ and below the value $y_{\rm trn}/(y_{\rm trn}+\beta_2)=\beta_1/(\beta_1+\beta_2)=0.75$ since $y_{\rm spk}<y_{\rm trn}$ for sufficiently small $0<\varepsilon\ll 1$. In fact, the transition with $\zeta=0.1$ is ended before $\delta_2=0.7155$: the attractor changes to a period-1 high frequency oscillation in variables x, y with z changing little. The simulations were done with Matlab. For technical reasons both y and z variables were rescaled by a factor 0.25, i.e., $y\to y/0.25$, $z\to z/0.25$.

V. CLOSING REMARKS

We have demonstrated that the dimensionless food chain model Eq. (2.3) admits chaotic dynamics at the singular limit $\zeta=0$, under the condition $\mathbf{z}<z_{\rm spk}\leqslant z_f\leqslant\bar{z}$ and with δ_2 above $y_{\rm spk}/(y_{\rm spk}+\beta_2)$ but within a range of order $1/\ln|\varepsilon|$. The period-doubling cascade is in the form of high-frequency oscillations. The mathematical mechanism responsible for the chaotic dynamics and their transitions is independent of ε, as long as it is sufficiently small $0<\varepsilon\ll 1$. The parameter range for which such complex dynamics take place contains an open neighborhood of the origin in β_1, δ_1, β_2. Notice that small β_is can be interpreted as predation efficiency. Although the parameter δ_1 is required to be small by our theoretical result, the phenomenon can still persist for moderate value of δ_1 as long as there is a unique junction-fold point on Σ. With increase in $\varepsilon>0$, which gives rise to a widened window in the period-doubling cascade bifurcation as implied by the main result, the range for δ_2 can also be small to produce chaotic dynamics.

We did not explore other parameter regions for chaotic dynamics and there are such regions but with chaos generating mechanisms different from what we discussed above. In fact our preliminary analysis shows that for the same parameter region $\underline{z}<z_{\rm spk}\leqslant z_f\leqslant\bar{z}$ but with δ_2 below β_0, the system can be chaotic by a mechanism exclusively due to the existence of the Pontryagin delay of stability at $z=\underline{z}$ for the intermediate predator subsystem. In addition, so long as $z_{\rm spk}<z^*$ and $y_f\approx y_{\rm spk}$ there should exist Shilnikov's saddle-focus homoclinic orbits[17,20] for parameter $0<\varepsilon<1$ not small but moderate. Also, in the region for which $\underline{z}<\bar{z}<z_{\rm spk}$ there exist the teacup attractors,[16,18,38] again for ε not near 0 but moderate. The chaos generating mechanism for the latter seems to enlist a *canard*.[35,36] All these cases can be treated by a similar approach of this paper. However, each case is complex enough that it should be dealt elsewhere. Also, we did not explore any biological significance of the period-doubling cascade considered here. That too should be dealt somewhere else.

ACKNOWLEDGMENTS

The author thanks Dr. S. Rinaldi for his constructive criticisms of the submitted draft. His input made a tremendous improvement possible for this paper in print. The author also thanks his colleague Dr. G. Hines for her valuable comments throughout the preparation of the manuscript.

APPENDIX

To find a parameter region in which the relation (3.6) holds, we consider instead a closely related region as follows:

$$\Lambda:=\{(\beta_1,\beta_2,\delta_1):\underline{z}<z_{\rm trn}<\bar{z}\},\tag{A1}$$

where the z values are summarized as follows, see also Fig. 2:

$$\begin{aligned}
&\underline{p}=(\underline{x},\underline{y},\underline{z})=\left(1,0,\left(\frac{1}{\beta_1+1}-\delta_1\right)\beta_2\right),\\
&p_{\rm trn}=(x_{\rm trn},y_{\rm trn},z_{\rm trn})\\
&\quad=(1-\beta_1,\beta_1,(1-\beta_1-\delta_1)(\beta_1+\beta_2)),\\
&\bar{p}=(\bar{x},\bar{y},\bar{z})=\left(\frac{1-\beta_1}{2},\frac{(1+\beta_1)^2}{4},\left(\frac{1-\beta_1}{1+\beta_1}-\delta_1\right)\right.\\
&\qquad\left.\times\left(\beta_2+\frac{(1+\beta_1)^2}{4}\right)\right).
\end{aligned}\tag{A2}$$

We note that to derive the z values above, we used the function

$$z=\psi(x,y):=\left(\frac{x}{\beta_1+x}-\delta_1\right)(\beta_2+y)$$

which solves the y-nullcline $g(x,y,z)=0$, and is nonnegative for $x\geqslant x_*:=\delta_1\beta_1/(1-\delta_1)>0$. Since all the points $\underline{p}$, $p_{\rm trn}$, $\bar{p}$ are on the x-stable branch of the parabola $f=0$, we also used the function,

$$y=\phi(x):=(1-x)(\beta_1+x),$$

which solves the parabola $f(x,y)=0$ for $x\geqslant 0$. In what follows, the intersection of the two nullclines $f=0$, $g=0$ is denoted as

$$z=\gamma(x):=\psi(x,\phi(x)),\quad\text{for}\quad x_*\leqslant x\leqslant 1.$$

We now describe the parameter region Λ of (A1) by a sequence of Propositions.

Proposition 6.1: $\underline{z}<\overline{z}$ *if*

$$0<\beta_1<1, \quad 0<\delta_1<\frac{1-\beta_1}{1+\beta_1},$$

$$0<\beta_2<b_1(\beta_1,\delta_1):=\frac{(1-\beta_1-\delta_1(1+\beta_1))(1+\beta_1)^2}{8\beta_1}.$$

Proof: Because

$$\underline{z}=\left(\frac{1}{1+\beta_1}-\delta_1\right)\beta_2$$

and

$$\overline{z}=\left(\frac{1-\beta_1}{1+\beta_1}-\delta_1\right)\left(\beta_2+\frac{(1+\beta_1)^2}{4}\right).$$

Solving the inequality $\underline{z}<\overline{z}$ for β_2 gives rise to the stated inequalities. □

Proposition 6.2: If the condition $\underline{z}<\overline{z}$ *of Proposition 6.1 holds, then there is a unique critical point* $\overline{x}<x^*<1$ *for* $z=\gamma(x)$ *and it is the absolute maximum in the interval* $\overline{x}\leqslant x\leqslant 1$. *In particular,* $\underline{z}<\overline{z}<z^*=\gamma(x^*)$.

Proof: Recall that

$$\gamma(x)=\left(\frac{x}{\beta_1+x}-\delta_1\right)(\beta_2+(1-x)(\beta_1+x)),$$

$$\text{for } \overline{x}=\frac{1-\beta_1}{2}\leqslant x\leqslant 1.$$

So it suffices to show γ has a unique critical point in the interval and it is a maximum point. To this end, we calculate

$$\gamma'(x)=\frac{1}{(\beta_1+x)^2}\{\beta_1\beta_2+[(1-\delta_1)(1-2x)+\delta_1\beta_1]$$

$$\times(\beta_1+x)^2\}:=\frac{Q(x)}{(\beta_1+x)^2}.$$

Hence it suffices to show that the cubic polynomial $Q(x)$ is monotone decreasing and has a unique root in $[\overline{x},1]$, or equivalently $Q'(x)<0, x\in(\overline{x},1), Q(\overline{x})>0$, and $Q(1)<0$. Calculating the derivative, we have

$$Q'(x)=2(\beta_1+x)[(1-\delta_1)(1-\beta_1-3x)+\delta_1\beta_1]$$

$$<0 \text{ for } \overline{x}<x<1 \text{ and } 0<\delta_1<\frac{1-\beta_1}{1+\beta_1}.$$

We have also

$$Q(\overline{x})=\beta_1\beta_2+[(1-\delta_1)\beta_1+\delta_1\beta_1](\beta_1+\overline{x})^2>0.$$

To show

$$Q(1)=\beta_1\beta_2+[-(1-\delta_1)+\delta_1\beta_1](\beta_1+x)^2<0,$$

we use the condition $\underline{z}<\overline{z}$. In fact, we can rewrite

$$0<\overline{z}-\underline{z}=\frac{-Q(1)-3\beta_1\beta_2-\beta_1(1+\beta_1)^2}{4(1+\beta_1)},$$

which implies what we wanted as $Q(1)<-3\beta_1\beta_2-\beta_1(1+\beta_1)^2<0$. □

Proposition 6.3: If the condition $\underline{z}<\overline{z}$ *of Proposition 6.1 holds, then*

$$\underline{z}<z_{\text{spk}}<z_{\text{trn}}.$$

Proof: In fact, by Proposition 6.2, $z=\gamma(x)$ is increasing in $[\overline{x},x^*]$ and decreasing in $[x^*,1]$. Thus, $\underline{z}=\gamma(1)$ is the absolute minimum since $\overline{z}=\gamma(\overline{x})>\underline{z}$ by assumption and $\underline{z}<z_{\text{trn}}=\gamma(x_{\text{trn}})$ follows automatically since $x_{\text{trn}}=1-\beta_1\in(\overline{x},1)=((1-\beta_1)/2,1)$. Similar, because y_{spk} is between the $\underline{y}=0$ and y_{trn}, the monotonicity also implies $\underline{z}<z_{\text{spk}}<z_{\text{trn}}$.

Proposition 6.4: Suppose the condition $\underline{z}<\overline{z}$ *of Proposition 6.1 holds. Then the condition*

$$z_{\text{trn}}<\overline{z}$$

holds if

$$0<\beta_1<\tfrac{1}{3}, \quad 0<\delta_1<\frac{1-3\beta_1}{1-\beta_1},$$

and

$$0<\beta_2<{}_2(\beta_1,\delta_1)$$

$$:=\frac{1+\beta_1}{\beta_1(1-\beta_1)}\left[\left(\frac{1-\beta_1}{1+\beta_1}-\delta_1\right)\frac{(1+\beta_1)^2}{4}\right.$$

$$\left.-(1-\beta_1-\delta_1)\beta_1\right].$$

Proof: Recall that

$$z_{\text{trn}}=(1-\beta_1-\delta_1)(\beta_1+\beta_2).$$

One solves formally for β_2 from the equation $z_{\text{trn}}<\overline{z}$ as follows:

$$\beta_2<b_2(\beta_1,\delta_1)=\frac{1+\beta_1}{\beta_1(1-\beta_1)}\left[\left(\frac{1-\beta_1}{1+\beta_1}-\delta_1\right)\frac{(1+\beta_1)^2}{4}\right.$$

$$\left.-(1-\beta_1-\delta_1)\beta_1\right]$$

$$:=\frac{1+\beta_1}{\beta_1(1-\beta_1)}\theta(\beta_1,\delta_1).$$

It is straightforward to check the following:

$$\frac{\partial\theta}{\partial\delta_1}(\beta_1,\delta_1)=-\frac{(1-\beta_1)^2}{4}<0,$$

$$\theta(\beta_1,0)=\frac{1-\beta_1}{4}(1-3\beta_1),$$

and

$$\theta(\beta_1,\delta_1)=0 \quad \text{if } \delta_1=\frac{1-3\beta_1}{1-\beta_1}.$$

Therefore, $\delta_1>0$ and $0<\beta_2<b_2(\beta_1,\delta_1)$ if $\beta_1<1/3, 0<\delta_1<(1-3\beta_1)/(1-\beta_1)$. We note that $0<\delta_1<(1-3\beta_1)/(1-\beta_1)$ automatically implies $0<\delta_1<(1-\beta_1)/(1+\beta_1)$. □

Summarizing the results above, we have

Proposition 6.5: $\underline{z}<z_{\text{trn}}<\overline{z}$ *if*

$$0<\beta_1<\tfrac{1}{3},\quad 0<\delta_1<\frac{1-3\beta_1}{1-\beta_1},$$

$$0<\beta_2<b(\beta_1,\delta_1):=\min\{b_1(\beta_1,\delta_1),b_2(\beta_1,\delta_1)\},$$

with b_1 as in Proposition 6.1 and b_2 as in Proposition 6.4. And $z<z_{\rm spk}<\bar{z}$ as required in (4.1) and (3.6).

Notice the following fact for Eq. (3.4) that defines the Pontryagin turning point $y=y_{\rm spk}$. When $\varepsilon=0$ and $\delta_1=0$, the denominator of the integrant is $\xi g(0,\xi,z)=\xi(-z/(\beta_2+\xi))$. Thus the $y_{\rm spk}$-defining equation becomes

$$-\frac{1}{z}\int_{y_{\rm spk}}^{\bar{y}}\frac{(\beta_2+\xi)f(0,\xi)}{\xi}d\xi$$
$$=0 \quad \text{if} \quad \int_{y_{\rm spk}}^{\bar{y}}\frac{(\beta_2+\xi)f(0,\xi)}{\xi}d\xi=0,$$

an equation independent of z. Therefore, we can conclude that for $\varepsilon=\delta_1=0$ the junction curve Σ is a line parallel to the z-axis and lies below the line $\{x=x_{\rm trn}=\phi^{-1}(y_{\rm trn}),y=y_{\rm trn}=\beta_1\}$ on the parabola $f=0$. Thus, Σ must intersect the curve $\gamma=\{g=0,f=0\}$ at a point called $p_{\rm spk}=(x_{\rm spk},y_{\rm spk},z_{\rm spk})$. [If it is clear from the text, we will not make the distinction between $y_{\rm spk}$ which is for the curve of Pontryagin's delay of lost stability $y=y_{\rm spk}(c)$ parameterized by a variable c diffeomorphically related to the z-coordinate of points on Σ and $y_{\rm spk}$ which is for the y-coordinate of the point $p_{\rm spk}$.] By the properties of γ and the parabola x-nullcline surface $f=0$, we can conclude that the intersection is unique and transversal. More importantly, we have the following result:

Proposition 6.6: For $0<\varepsilon\ll 1$ and $\delta_1>0$ small, the point $p_{\rm spk}=(x_{\rm spk},y_{\rm spk},z_{\rm spk})$ persists with the property that it is the unique point on the junction curve Σ over the bounded segment $0\leqslant z\leqslant z^*$ at which the reduced vector field on $f=0$ is tangent to Σ and changes its direction with respect to the junction curve, i.e., at points on opposite sides of $p_{\rm spk}$ on Σ the vector field points to opposite sides of Σ.

Proof: Note first that the junction curve Σ can be parameterized by the z variable for small $0\leqslant\varepsilon\ll 1$ and $0\leqslant\delta_1<0$. Thus in what follows, we will denote the junction curve by $x=\phi^{-1}(y),y=y_{\rm spk}(z,\varepsilon,\delta_1)$ in terms of the parameterization in $z\in[0,z^*]$. Denote the reduced vector field that is restricted on the curve Σ by $v(z,\varepsilon,\delta_1)$. Let $n(z,\varepsilon,\delta_1)$ denote a continuous normal vector of the junction curve and

$$m(z,\varepsilon,\delta_1)=\langle v,n\rangle$$

be the inner product of v and n. Then we already know that $m(z_{\rm spk},0,0)=0$. The persistence part of the result follows from the implicit function theorem if we can show that $(\partial/\partial z)\,m(z_{\rm spk},0,0)\neq 0$. To this end, we note first that since at $\varepsilon=\delta_1=0$, Σ is a line parallel to the z-axis, the normal vector n is a constant vector. So $(\partial/\partial z)\,m(z_{\rm spk},0,0)=\langle v',n\rangle$, where v' denotes the partial derivative of v in z at $z=z_{\rm spk}$ with $\varepsilon=\delta_1=0$. Expressing v in its components, we have

$$v=(D\phi^{-1}(y)$$
$$\times(yg(\phi^{-1}(y),y,z)),yg(\phi^{-1}(y),y,z),\varepsilon zh(y,z)).$$

Using the facts that at $\varepsilon=\delta_1=0$ the junction curve Σ is a line parallel to the z-axis, i.e., $y=y_{\rm spk}$ is independent of z, we have

$$v'=\frac{\partial v}{\partial z}(z,0,0)=\left(-D\phi^{-1}(y)\frac{y}{\beta_2+y},-\frac{y}{\beta_2+y},0\right).$$

Because $n(z,0,0)$ is a normal vector to Σ that is also on the tangent space of the parabola $f=0$,

$$n(z,0,0)=(D\phi^{-1}(y)b,b,0)$$

for some nonzero constant b. Putting these facts together, we have that at $\varepsilon=\delta_1=0$ and $z=z_{\rm spk}$,

$$\frac{\partial}{\partial z}m(z_{\rm spk},0,0)=\langle v',n\rangle$$
$$=-(D\phi^{-1}(y)^2+1)b\frac{y}{\beta_2+y}\neq 0.$$

This proves the persistence of $p_{\rm spk}$ for small $\varepsilon>0$ and $\delta_1>0$. Using the fact that the reduced vector field is transversal to Σ at any other point over the compact segment $\Sigma\cap\{0\leqslant z\leqslant z^*\}$, pointing down for $z>z_{\rm spk}$ and up $z>z_{\rm spk}$, the uniqueness of point $p_{\rm spk}$ follows in the compact interval. □

Recall the definition of the Poincaré return map π defined in the text. The main result of this paper is as follows:

Theorem 6.1: *At $\zeta=0$ and for sufficiently small $0<\varepsilon\ll 1$ and $0<\delta_1$, there exists a one-dimensional Poincaré return map π for the limiting system of Eq. (2.3) under the conditions (3.6). This map undergoes a reversed period-doubling cascade to chaos for δ_2 within an $\mathcal{O}(1/|\ln\varepsilon|)$ above $\beta_0=y_{\rm spk}/(y_{\rm spk}+\beta_2)$.*

Proof: The existence and smoothness of the return map π is established in the main text. We only need to prove that it goes through a reversed period-doubling cascade of bifurcations within the range $\delta_2-\beta_0=\mathcal{O}(1/|\ln\varepsilon|)$. The argument is similar to the proof of Theorem 1.1 of Ref. 11. The necessary modifications are as follows. First, we consider only the limiting case $\zeta=0$ not the full-fledged case $0<\zeta\ll 1$. Because of this, we do not need the smoothness of the fold $y=\bar{y}$ on $f=0$ nor the smoothness of the x-nullcline manifold $\{f=0\}\cup\{x=0\}$ along the transcritical line $y=y_{\rm trn}$ as required for the hypotheses **H.1–H.4** of Theorem 4.1 of Ref. 11. The smoothness of these turning points are required only for the persistence argument of Theorem 1.1, Lemma 3.2, and Theorem 4.1 for $0<\zeta\ll 1$. It is not needed for the limiting return map. Therefore the part of proof of Theorem 1.1 that is for the limiting map applies with one modification left. This modification again has to do with the type of turning point for the (y,z)-dynamics. In the Ref. 11 case, the turning point labeled (C_2,V_2) in Fig. 5.1 of Ref. 11 is again a differentiable saddle-node type. In contrast, the turning point p of Eq. (2.3) is of Pontryagin's type. However, this type of turning point or the saddle-node type considered in Ref. 11 has no effect on the *topology* of kneading sequence calculations of Sec. 5.3 in Ref. 11. The estimate that the period-doubling cascade takes place within an interval of $\delta_2-\beta_0=\mathcal{O}(1/|\ln\varepsilon|)$ depends only on the existence of the junction-fold point $p_{\rm spk}$ on the junction line Σ at which there

is a limiting homoclinic orbit to it at $\varepsilon = 0$. Specifically, see the proof of Theorem 1.2 about the derivation part for the bifurcation value of y_f (which is equivalent to ϱ in Ref. 11) at which the critical point p_{spk} is mapped to itself by the return map. □

We end this appendix by pointing out that the theorem can be extended to any $0 < \delta_1 < 1$ so long as the conclusion of Proposition 6.6 is satisfied, that is, the existence of a unique junction-fold point on Σ.

[1] B. Deng, ''Glucose-induced period-doubling cascade in the electrical activity of pancreatic β-cells,'' J. Math. Biol. **38**, 21–78 (1999).
[2] S.L. Pimm, *Food Webs* (Chapman and Hall, New York, 1982).
[3] R. May, ''Simple mathematical models with very complicated dynamics,'' Nature (London) **261**, 459–467 (1976).
[4] P. Hogeweg and B. Hesper, ''Interactive instruction on population interactions,'' Comput. Biol. Med. **8**, 319–327 (1978).
[5] M.E. Gilpin, ''Spiral chaos in a predator–prey model,'' Am. Nat. **113**, 306–308 (1979).
[6] C. Elton and M. Nicholson, ''The ten-year cycle in numbers of the lynx in Canada,'' J. Anim. Ecol. **11**, 215–244 (1942).
[7] F. Takens, ''Detecting strange attractors in turbulence,'' Lect. Notes Math. **898**, 366–381 (1981).
[8] W.M. Schaffer, ''Stretching and folding in lynx fur returns: Evidence for a strange attractor in nature?'' Am. Nat. **124**, 798–820 (1984).
[9] O.E. Rössler, ''Chaotic behavior in simple reaction systems,'' Z. Naturforsch. **31**, 259–264 (1976).
[10] S. Ellner and P. Turchin, ''Chaos in a noisy world: New methods and evidence from time-series analysis,'' Am. Nat. **145**, 343–375 (1995).
[11] B. Blasius, A. Huppert, and L. Stone, ''Complex dynamics and phase synchronization in spatially extended ecological systems,'' Nature (London) **399**, 354–359 (1999).
[12] O. De Feo and S. Rinaldi, ''Yield and dynamics of tritrophic food chains,'' Am. Nat. **150**, 328–345 (1997).
[13] O. De Feo and S. Rinaldi, ''Top-redator abundance and chaos in tritrophic food chains,'' Ecology Lett. **2**, 6–10 (1999).
[14] A.J. Lotka, *Elements of Physical Biology* (Williams and Wilkins, Baltimore, 1925).
[15] V. Volterra, ''Fluactuations in the abundance of species, considered mathematically,'' Nature (London) **118**, 558–560 (1926).
[16] A. Hastings and T. Powell, ''Chaos in a three-species food chain,'' Ecology **72**, 896–903 (1991).
[17] K. McCann and P. Yodzis, ''Bifurcation structure of a three-species food chain model,'' Theoretical population biology **48**, 93–125 (1995).
[18] Yu.A. Kuznetzov and S. Rinaldi, ''Remarks on food chain dynamics,'' Math. Biosci. **134**, 1–33 (1996).
[19] M.P. Boer, B.W. Kooi, and S.A.L.M. Kooijman, ''Homoclinic and heteroclinic orbits to a cycle in a tri-trophic food chain,'' J. Math. Biol. **39**, 19–38 (1999).
[20] Yu.A. Kuznetzov, O. De Feo, and S. Rinaldi, ''Belyakov homoclinic bifurcations in a tritrophic food chain model,'' SIAM J. Appl. Math. (to be published).
[21] M. Feigenbaum, ''Quantitative universality for a class of nonlinear transformations,'' J. Stat. Phys. **19**, 25–52 (1979).
[22] E.F. Mishchenko, Yu.S. Kolesov, A.Yu. Kolesov, and N.Kh. Rozov, *Asymptotic Methods in Singularly Perturbed Systems*, *Monographs in Contemporary Mathematics* (Consultants Bureau, New York, 1994).
[23] B. Deng, ''Constructing homoclinic orbits and chaotic attractors,'' Int. J. Bifurcation Chaos Appl. Sci. Eng. **4**, 823–841 (1994).
[24] B. Deng, *Folding at the Genesis of Chaos in Proceedings of the First World Congress of Nonlinear Analysts* (Walter de Gruyter, Berlin, 1996), Vol. IV, pp. 3765–3777.
[25] M.L. Rosenzweig and R.H. MacArthur, ''Graphical representation and stability conditions of predator–prey interactions,'' Am. Nat. **97**, 209–223 (1963).
[26] C.S. Holling, ''Some characteristics of simple types of predation and parasitism,'' Can. Entomologist **91**, 385–398 (1959).
[27] S. Muratori and S. Rinaldi, ''Separation condition for the existence of limit cycles in slow-fast systems,'' Appl. Math. Modeling **15**, 312–318 (1991).
[28] S. Rinaldi and S. Muratori, ''Slow-fast limit cycles in predator–prey models,'' Ecol. Model. **61**, 287–308 (1992).
[29] L. Lenbury and C. Likasiri, ''Low- and high-frequency oscillations in a food chain where one of the competing species feeds on the other,'' Math. Comput. Modelling **20**, 71–89 (1994).
[30] O. De Feo and S. Rinaldi, ''Singular homoclinic bifurcations in tritrophic food chains,'' Math. Biosci. **118**, 7–20 (1998).
[31] L.C. Pontryagin, ''Asymptotic behavior of solutions of systems of differential equations with a small parameter at higher derivatives,'' Izv. Akad. Nauk. SSSR Ser. Math. **21**, 605–626 (1957) (in Russian).
[32] S. Schecter, ''Persistent unstable equilibria and closed orbits of a singularly perturbed equation,'' J. Diff. Eqns. **60**, 131–141 (1985).
[33] D. Terman, ''The transition from bursting to continuous spiking in excitable membrane models,'' J. Nonlinear Sci. **2**, 135–182 (1992).
[34] B. Deng, ''Homoclinic twisting bifurcations and cusp horseshoe maps,'' J.D.D.E. **5**, 417–467 (1993).
[35] E. Benoit, J. L. Callot, F. Diener, and M. Diener, ''Chasse au canards,'' Collect. Math. **31**, 37–119 (1981).
[36] W. Eckhaus, ''Relaxation Oscillations Including a Standard Chase on French Ducks,'' in *Asymptotic Analysis II*, Springer Lecture Notes Math. (Springer, Berlin, 1983), Vol. 985, pp. 449–494.
[37] P. Collet and J.-P. Eckmann, *Iterated Maps of Interval as Dynamical Systems* (Birkhauser, New York, 1980).
[38] S. Muratori and S. Rinaldi, ''Low- and high-frequency oscillations in three-dimensional food chain system,'' SIAM (Soc. Ind. Appl. Math.) J. Appl. Math. **52**, 1688–1706 (1992).